Circular cylinder drag reduction by three-electrode plasma actuators

Journal of Physics: Conference Series **166** (2009) 012015 doi:10.1088/1742-6596/166/1/012015

Circular cylinder drag reduction by three-electrode plasma actuators

R Sosa, J D'Adamo and G Artana

Laboratorio de Fluidodinámica, Universidad de Buenos Aires, Av. Paseo Colon 850, C1063ACV, Buenos Aires, Argentina. CONICET

rsosa@fi.uba.ar

Abstract. The drag reduction in a circular cylinder was explored by means of a novel three electrode plasma actuator (*DBDE*). The *DBDE* actuator can reduce the drag coefficient up to a ~25% respect to the base flow drag coefficient. It has been demonstrated that, within the present experimental conditions, the *DBDE* actuator, for a fixed value of the power coefficient, adds a higher momentum to the flow and, consequently, produces a higher drag reduction than the *DBD* actuator with the same power coefficient. The actuator efficiency was analysed in terms of the momentum added to the flow revealing similar behaviour for both kind of actuators. However to produce similar levels of actuation both kind of actuators require different values of V_{AC} voltages that resulted always lower for *DBDE*. The reduction in this high voltage value is highly beneficial as is directly related to: a lower HV AC source power requirement, a reduction in the dielectric breakdown probability of the device and a reduction in leakage currents.

1. Introduction

Flow over bluff bodies, for Reynolds number exceeding a critical value, presents vortex shedding in the wake hence resulting in a significant pressure drop on the rear surface of the body. This vortex shedding occurs over a wide range of Reynolds numbers causing structural vibrations, acoustic noise and resonance, enhanced mixing, and significant increases in the aerodynamic drag.

Active flow control techniques have been studied to improve aerodynamic performance of bluff bodies. Most of the flow actuation techniques are concentrated on the reattachment of separated flow which results in enhancing lift and/or reducing drag forces. Flow reattachment can be achieved using surface blowing to construct a pseudo streamline-shaped surface [1-2], surface suction to obtain a thinner boundary layer [3], oscillations of the body (rotary [4-5], streamwise [6] and transverse [7-8]) or synthetic jets [9-10] to utilise the effects of momentum injection into a boundary layer. However, these techniques add different kind of complexity to the system and offer in general a limited controllability in eliminating or delaying flow separation.

Recently, the use of plasma actuators has been proposed as an alternative method to control flow separation (see for instance the comprehensive review [11]). These plasma actuators use a non-thermal surface plasmas and the flowing air close to the surface of the body is ionized. As a consequence of the elastic collisions between the migrating charged particles and the neutral species of the gas, the neutrals increase their momentum giving rise to an 'electric wind' that takes place in the close vicinity of the wall surface. This additional body force resulting from the strong directional ion flow can

suppress flow separation as it can be used to overcome the destabilising adverse pressure gradient. Also other mechanisms like alterations of the physical properties of the gas (density, viscosity, etc), may eventually contribute to enhance the electromechanical coupling of discharge-airflow [12-13]. The plasma actuators are technologically attractive because of their simplicity (they have no moving parts) and their very short response time (typically of the order of tens of milliseconds, see for instance [11]).

Plasma actuators can be classified considering the number of electrodes comprised and their arrangement. A first group involves devices employing two electrodes arrangements. At the same time this actuators group may be divided if we consider devices in which the electrodes are separated by a dielectric barrier, usually known as dielectric barrier discharge actuators (*DBD*), or devices in which the two electrodes are bared and flush mounted on a dielectric surface (*BED*).

The *DBD* actuators use periodically excited electrodes and the dielectric barrier interposed between them plays an important role in the stabilisation of the discharge. A large number of aerodynamic studies of flows actuated with *DBD* have been carried out (see for instance [14-19]). Typically, the *DBD* actuator can generate an electric wind with a velocity up to about $8ms^{-1}$. Nevertheless the plasma area extension is limited as the ionization may extend up to ~2 cm from the electrode edge. This might be a crucial drawback for large scale applications.

The *BED* actuators may produce distinctive gaseous discharges depending on the applied potential and the flow conditions [20], these are: unipolar coronas discharge (*UC*), bipolar coronas (*BC*) and plasma sheet discharge (*PS*). In any case the electrodes excitation is produced either with DC or with a periodic voltage supply. The aerodynamic performances of *BED* plasma actuators have been reported in previous works for different flow conditions [21-27].

The main drawback of *BED* plasma actuators is that the electrical discharge may become rather unstable under certain atmospheric conditions. For instance, corona-to-arc transition have been detected in some cases when the relative air humidity exceeded a threshold of about 55% [28].

More recently [29], a new group of plasma actuators consisting in three electrodes devices has been developed (*TED*). Figure 1 shows the arrangement where two electrodes are flush mounted on the air exposed surface (upper electrodes (1) and (3)), and a third one is placed on the opposite side of the insulating surface (lower electrode, (2)). If the electrode (3) and the electrode (2) are grounded biased while the upper electrode (1) is at an AC voltage a typical surface dielectric barrier discharge is formed between electrodes (1) and (2), as is schematically showed in figure 1a. In this case the *TED* actuator works like a conventional *DBD* actuator.

On the other hand when the electrode (1) is at an AC voltage and a high enough DC voltage is applied to the electrode (3) one can produce different discharges, depending on the polarity of the DC voltage (V_{DC}). Thus for $V_{DC} < 0$ a luminescent plasma sheet (named sliding discharge, *SD*) that occupies the whole electrode gap is produced (see figure 1c), and if $V_{DC} > 0$ a discharge that visually looks like a *DBD* (see figure 1b), but with different electrical and mechanical characteristics, is established. Both discharge regimes are as stable as the *DBD* discharge and have the advantage that they allow large-scale applications because the discharge extension may be increased up to the gap between electrodes (1) and (3) [30-32].

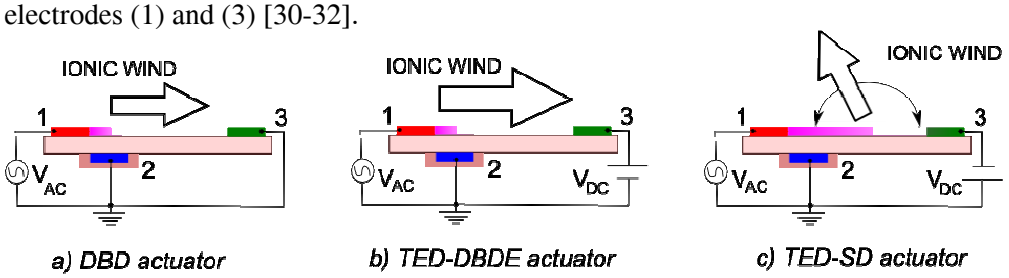

a) DBD actuator b) TED-DBDE actuator c) TED-SD actuator

Figure 1. Different plasma actuators. a) Dielectric Barrier Discharge actuator (*DBD*), b) Three Electrode Device with $V_{DC} > 0$ (*TED-DBDE*), c) Three Electrode Device with $V_{DC} < 0$ (*TED-SD*)

In the *TED* actuators the induced electric wind morphology is strongly dependent on the polarity of the DC voltage applied to electrode (3). When $V_{DC} < 0$, and the sliding discharge (*SD*) takes place, two induced jet flows, with origin at the electrodes proximity, result directed towards the inter-electrode space. In this case the global induced flow direction also dependent on the applied AC voltage. By varying the AC voltage value the global plume like flow direction and span angles almost lying in the range 0-180º referred to the dielectric surface (see figure 1c). More detailed experiments concerning induced flow by the *SD* actuator can be found in [32].

On the other hand if we consider a *TED* actuator with a positive DC component applied to electrode (3) the induced electric wind direction (figure 1b) is coincident with that observed in a single *DBD* actuator (figure 1a) but the positive DC voltage allowed to increase the induced electric wind, respect to the case $V_{DC} = 0$, without a noticeable increase in the electrical power consumption [31]. This last configuration will be referred as enhanced dielectric barrier discharge or *DBDE* actuator.

The objective of this work is to determine the capability of *DBDE* plasma actuators to reduce the aerodynamic drag experienced by a circular cylinder in uniform translation. We are especially interested in comparing, for this flow configuration, the performance of the *DBDE* actuation with the more traditional *DBD* ones [33-35].

To undertake this analysis we performed two different set of experiments. One of them has as objective to characterise the induced electric wind when the plasma actuator is applied in quiescent air. We focus our attention in the difference between the cases $V_{DC} = 0$ (*DBD*) and $V_{DC} > 0$ (*DBDE*). This set of experiments were done mounting the plasma actuator on a flat plate in order to simplify the measurement of the induced velocity. Electrical measurements complete this study. In a second set of experiments we analyse the modifications produced in the aerodynamic drag exerted on a circular cylinder (within the Re range of $6.10^3 < Re < 13.10^3$) by either *DBD* or *DBDE* actuators.

2. Experimental set-up

2.1. Induced flow in quiescent air and electrical measurements

A scheme of the experimental set up is shown in figure 2. In order to analyse the induced electric wind in a quiescent air the plasma actuator was mounted in a dielectric flat plate.

In this case the electrode arrangement consisted in two flat aluminium foils (electrodes (1) and (3)) flush mounted on the surface of a polymethyl methacrylate flat plate (150 mm x 350 mm, thickness of 3 mm) and a third one disposed at the opposite side (electrode (2)). Electrode (2) was buried in order to inhibit discharges on this dielectric plate side. The electrodes dimensions are 50 μm thickness, length 300 mm (in the z direction, see figure 2) and width 5 mm. The inter-electrode gap between electrodes (1) and (3) was 28 mm.

A variable DC power supply (V_{DC} in the range +10 ÷ +20 kV, 10 W) biased positively electrode (3). Another variable AC sine voltage power supply (frequency: f = 8 kHz, zero mean value; peak to peak voltage V_{AC} up to 20 kV) was applied to electrode (1). The AC power supply consisted in a function generator coupled to an audio amplifier (of 150 watt) that fed a high voltage transformer coil [36]. The electric current flowing in the system, $I_2(t)$ and $I_3(t)$, were measured with shunt resistances ($R = 50\Omega$) connected to an oscilloscope with 60 MHz of analogical bandwidth and 1Gs/s of sampling rate. The AC voltage applied to electrode (1), and the DC voltage applied to electrode (3) were measured with a HV probe (1000 × / 3.0 pF / 100MΩ).

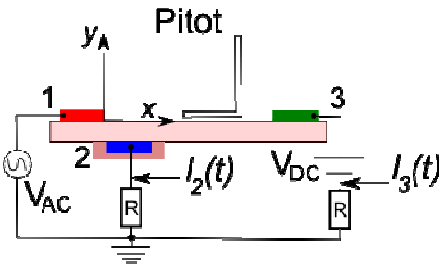

Figure 2. Experimental set-up for measure the induced electric wind in a quiescent air and the actuators electrical characteristics

The set-up was placed horizontally in the test section of a low speed wind tunnel with a square test section of 450 mm x 450 mm (850 mm length) in order to avoid external flow perturbations.

One pressure probe (Pitot tube in figure 2) was mounted on the dielectric surface, placed in front of electrode (1) at x = 15 mm, and y = 0.48 mm. This probe was made of electrically insulating glass tube (internal diameter: ID = 0.97 mm, outer diameter OD = 1.3 mm) and was connected by mean of a tygon tube to a low differential pressure transmitter (0 to 30 Pa, accuracy of 0.4% full scale). The reference pressure value was measured at the test section but far away from the electrodes.

2.2. Aerodynamic drag measurement

In this study the electrodes were mounted on a PMMA cylinder that was 40 mm in diameter D (length L = 300 mm). The cylinder was a hollow tube with a 3-mm thick wall.

The electrode arrangement consists in three electrodes flush-mounted on the cylinder surface (two couple electrodes (1)-(2) and one electrode (3), see figure 3a). The electrodes dimensions were 50 µm thickness, length 300 mm (in the z direction) and width 5 mm. All the electrodes were parallel to the cylinder axis (see figure 3a) and the inter-electrode gap between electrodes (1) and (3) was 28 mm.

Our experimental device was placed in an open low speed wind tunnel (0-5 m/s) with a square test section of 450 mm x 450 mm (850 mm length) with the cylinder axis placed perpendicular to the main flow (U_0) and oriented such that the electrode (3) occupied the rear stagnation point (θ = 0) and the pairs of electrodes (1) and (2) occupied positions θ = 90º and θ = -90º respectively (see figure 3a).

We have measured the drag exerted on the cylinder by means of a balance that enable us to detect changes of 10 mN in the force. The cylinder was hanged from this balance by two supports (fixed on both cylinder ends through pieces of nylon entering in the hollows of the tube) and the force was detected by equilibrating the moment of the drag force with the moment of the weights of the balance. (an outline of the wind tunnel and aerodynamic drag balance is shown in figure 3b). The blockage ratio was 8.9% and no correction has been applied to the drag data for blockage effects.

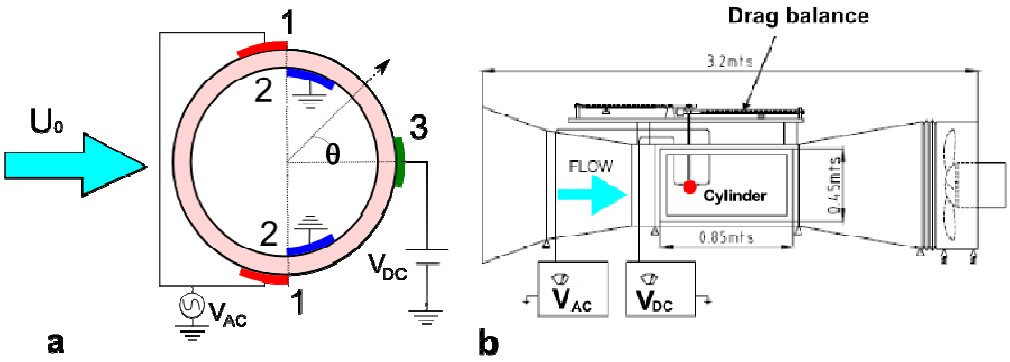

Figure 3. Experimental set-up for the aerodynamics measures. a) Detail of the *TED* actuator mounted on the cylinder, b) Scheme of the wind tunnel and aerodynamic balance

3. Results.

3.1. Induced electric wind and power consumption

The morphology of the induced flow in the case of the *DBD* actuator has been widely studied [19,37-39]. The *DBD* induces a depression above the right edge of electrode (1), and then the fluid is accelerated tangentially to the wall towards electrode (3). In the case of the three-electrode device actuator with $V_{DC} > 0$, it seems that the depression occurs above the whole discharge region, (i.e. between electrodes (1) and (3)). It was previously demonstrated that when a positive DC component is applied to electrode (3) the induced momentum increase, respect to the momentum induced by a *DBD* actuator (i.e. $V_{DC} = 0$), whatever the x position [31]. This increase also occurred downstream of the visible discharge extension. This behaviour was associated to alterations of the asymmetric character of the induced flow in the *DBD* actuators (the negative *DBD* discharge, occurring during the negative half cycle, resulted in a faster velocity than the positive one, [38]). The velocity increase when $V_{DC} > 0$ due to the acceleration of the negative space charge created by the *DBD* in the negative half-cycle results higher than the velocity reduction during the *DBD* positive half-cycle, producing a higher time-averaged velocity.

In the present work a single *DBDE* actuator has been mounted on a flat plate in order to characterise the induced flow in terms of the applied voltages (V_{DC} and V_{AC}) and the consumed electrical power (P). The same geometrical parameters that those considered for the cylinder flow control case have been used (i.e. dielectric thickness, electrodes dimensions and inter-electrode gap between electrodes (1) and (3)). For the flat plate tests we have measured the induced flow velocity at fixed point in all the considered cases to characterise the induced flow (complete velocity profiles can be found in [31]). For the *DBD* and *DBDE* actuators we will adopt the following nomenclature: DBD_I and DBD_IE_J, where the subscripts I and J indicate the applied V_{DC} and V_{AC} voltages respectively.

Figure 4 shows the velocity (U_j) measured at x = 15 mm and y = 0.48 mm versus V_{AC}, without the DC component (*DBD* actuator case) and with V_{DC} = +12 kV (named DBD_IE_{12}) and +16 kV (named DBD_IE16). This figure enables to show that the induced electric wind velocity increases with the applied DC component value.

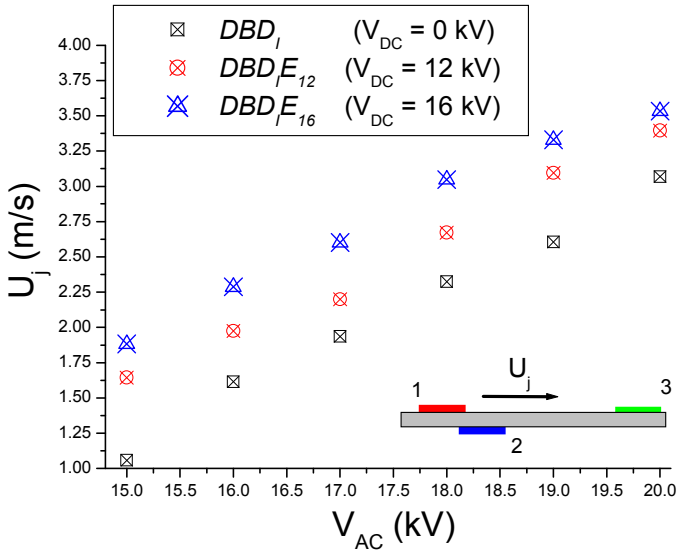

Figure 4. Induced flow velocity U_j vs. V_{AC} for different V_{DC} values

We also can observe that the same induced values of U_j observed for the *DBDE* actuator can be achieved with a *DBD* actuator but applying higher values of V_{AC}. For instance if we consider the *DBDE* actuator with V_{DC} = 16 kV and V_{AC} = 15 kV (named $DBD_{15}E_{16}$) the induced flow velocity results $U_j \approx 1.9$ m/s, and if we consider a single *DBD* actuator with V_{AC} = 17 kV (named DBD_{17}) the

induced velocity has been resulted almost the same. Bellow we will discuss what does this higher V_{AC} value mean in terms of the actuator electrical power consumption.

It is worth nothing that the upper limit for the V_{DC} value was ~16 kV because under our experimental conditions (i.e. electrodes radii and inter-electrode gap) an increase of V_{DC} beyond this upper limit will produce sparking between electrodes (1) and (3).

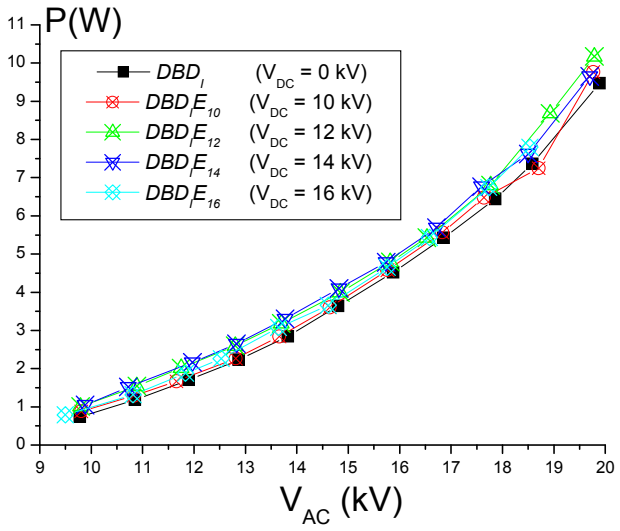

Figure 5. Electrical power consumption (*P*) as a function of V_{AC} with V_{DC} as a parameter for the *DBD* and *DBDE* actuators

Figure 5 shows the electrical power consumption (*P*) versus V_{AC}, for a single *DBD* actuator and for a single *DBDE* actuator considering several positive values of V_{DC}. It shows that for a fixed value of V_{AC} an increase in the applied V_{DC} value produce a slight increase in the electrical power consumption. For instance with V_{AC} = 15 kV, P ≈ 3.6 W for a single *DBD* (i.e. V_{DC} = 0, DBD_{15}) whereas $P \approx 4.1$ W for a single *DBDE* actuator with V_{AC} = 15 kV and V_{DC} = 16 kV ($DBD_{15}E_{16}$) resulting in a power consumption increase of ~12%. In general the increase in the electrical power consumption, with the increase in V_{DC}, was confined within the range ~5÷15%.

On the other hand we can observe that in all the cases the electrical power increases with V_{AC} according to a parabolic function $P = K(V_{AC} - V_0)^2$, been $K = 5.73 \times 10^{-8} \frac{W}{V^2}$ and $V_0 = 7.58 \times 10^3 V$ for the single *DBD* actuator under the present experimental conditions.

Now we can complete our comparison of performance of both kind of actuators, to induce a flow, considering energy consumption arguments. The analysis shows that although similar values of U_j can be achieved with both type of actuators the power consumption required by the *DBDE* actuator results always lower. For instance in the previously worked out example the *DBDE* actuator requires $P \approx 4.1$ W to induce a velocity of $U_j \approx 1.9$ m/s ($DBD_{15}E_{16}$) whereas to induce the same velocity the *DBD* actuator consumption is $P \approx 5.4$ W (DBD_{17}). This example shows that the *DBDE* requires only the ~76 % of the electrical power consumed by the *DBD* actuator to induce the same flow velocity. To reinforce this experimental observation Table 1 shows another examples comparing the consumed power of the *DBD* and *DBDE* actuators (P^{DBD} and P^{DBDE} respectively) to induce the same velocity U_j.

Table 1. Comparisons between the different actuators consumed power to induce the same velocity

U_j(m/s)	*DBD*		*DBDE* (V_{DC} = 16 kV)		P^{DBDE}/P^{DBD} (%)
	V_{AC} (kV)	P^{DBD} (W)	V_{AC} (kV)	P^{DBDE} (W)	
1.9	17	5.4	15	4.1	76
2.3	18	6.4	16	4.8	75
2.6	19	7.4	17	5.7	77
3.1	20	9.5	18	6.8	72

In conclusion the *DBDE* actuators requires less power consumption to produce the same induced flow velocity. In order to highlight this behaviour we will compare the actuators performance in terms of non-dimensional parameters. One of them is the non-dimensional momentum coefficient (C_μ), defined as:

$$C_\mu = \frac{{U_j}^2 b}{{U_0}^2 D} \tag{1}$$

Where b is the characteristic height of the jet induced by the plasma actuator. The momentum coefficient evaluates the ratio between plasma actuator added momentum ($\propto \rho {U_j}^2 bL$) and a characteristic momentum flow in the free stream ($\propto \rho {U_0}^2 DL$). Another important parameter will be the power coefficient (C_W) defined as:

$$C_W = \frac{P}{\frac{1}{2}\rho U_0^3 LD} \tag{2}$$

The power coefficient evaluates the ratio between the plasma actuator consumed electric power (P) and a characteristic flow of kinetic energy in the free stream flow.

Figure 6 shows the DBD_I and DBD_IE_{16} (*DBDE* with V_{DC} = 16 kV) momentum coefficient (C_μ) as a function of the power coefficient (C_W) for different *Re* numbers ($\mathrm{Re} = U_0 D/\nu$).

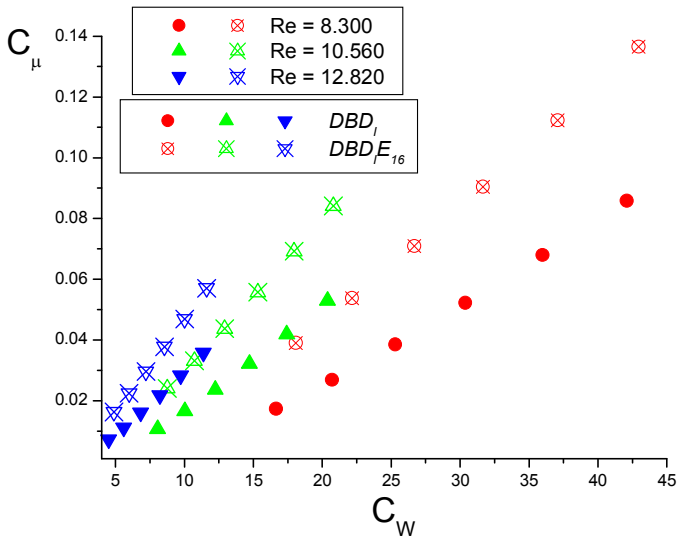

Figure 6. DBD_I and DBD_IE_{16} (*DBDE* with V_{DC} = 16 kV) momentum coefficient (C_μ) as a function of the power coefficient (C_W) for different *Re* numbers

We can observe that for the same non-dimensional power coefficient the momentum addition to the flow is higher if we consider a *DBDE* actuators rather than a *DBD* ones. This last behaviour was observed for all the considered *Re* numbers.

3.2. Aerodynamic drag force

Figure 7 shows the drag force (F_D) as a function of the free stream velocity (U_0) for the base flow (i.e. without discharge) and for the flow modified by means of two single *DBD* actuators considering different V_{AC} values. It can be observed that a significant drag reduction can be achieved by means of the *DBD* actuation. Moreover, if the V_{AC} value increase the drag reduction is higher. Typically the *DBD* actuation can reduce the drag force within ~15÷25% for all the free stream velocity tested values.

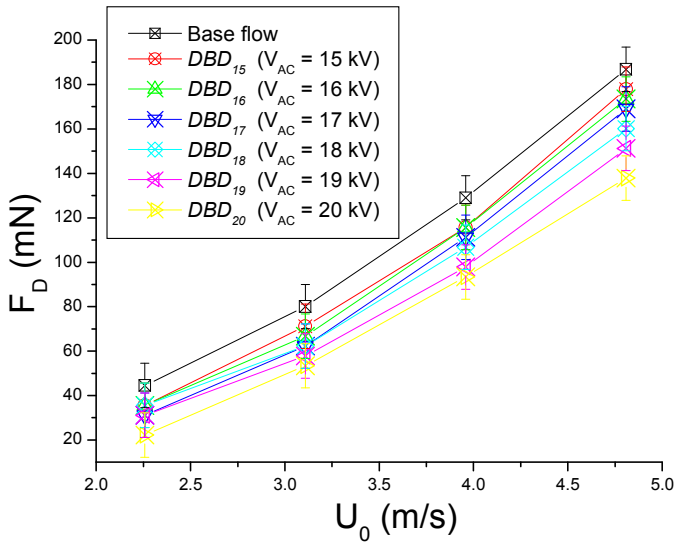

Figure 7. Drag force (F_D) as a function of the free stream velocity (U_0) for the base flow and for the flow modified by means of *DBD* actuators

In order to compare the drag reduction achieved with the different kind of actuators Figure 8 shows the drag force (F_D) as a function of the free stream velocity (U_0) for the base flow (i.e. without discharge) and for the flow modified either by two single *DBD* or *DBDE* actuators. The values of V_{DC} and V_{AC} were chosen such as the induced wind velocity (U_j) in quiescent air result almost the same for both kind of actuators in each figure. So figure 8a compare the case of *DBD* actuators with V_{AC} = 17 kV (DBD_{17}) with the case of *DBDE* actuators with V_{AC} = 15 kV and V_{DC} = 16 kV ($DBD_{15}E_{16}$), and figure 8b compare the case of *DBD* actuators with V_{AC} = 18 kV (DBD_{18}) with the case of *DBDE* actuators with V_{AC} = 16 kV and V_{DC} = 16 kV ($DBD_{16}E_{16}$).

It is clear from figures 8a y 8b that if we adjust the actuators parameters (i.e. V_{AC} and V_{DC} values) in order to induce the same flow velocity we produce almost the same drag reduction on the cylinder whatever the actuator used.

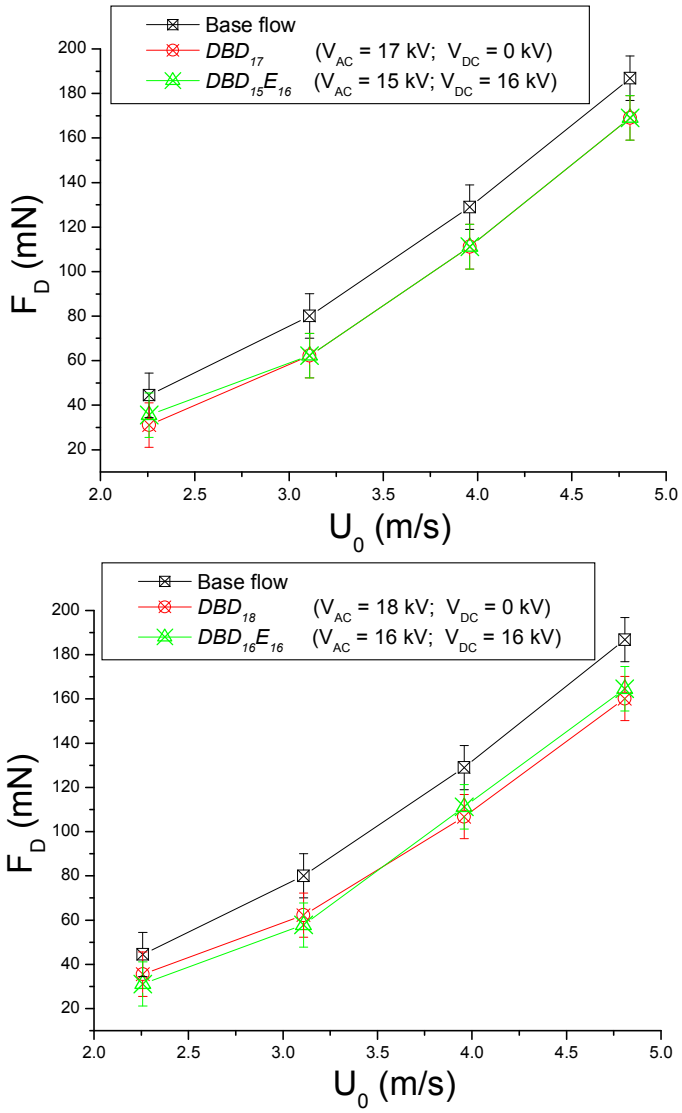

Figure 8. Drag force (F_D) as a function of the free stream velocity (U_0) for the base flow and for the flow modified by means of: upper) *DBD* actuators (V_{AC} = 17 kV and V_{DC} = 0 kV) and *DBDE* actuators (V_{AC} = 15 kV and V_{DC} = 16 kV); lower) *DBD* actuators (V_{AC} = 18 kV and V_{DC} = 0 kV) and *DBDE* actuators (V_{AC} = 16 kV and V_{DC} = 16 kV);

It is useful to compare both kind of actuators considering the drag force in its non dimensional form (i.e. the drag coefficient, C_D):

$$C_D = \frac{F_D}{\frac{1}{2}\rho U_0^{\,2} DL} \tag{3}$$

Figure 9 shows the drag coefficient (C_D) as a function of the power coefficient (C_W) for the *DBD* and *DBDE16* actuators considering two different Reynolds numbers.

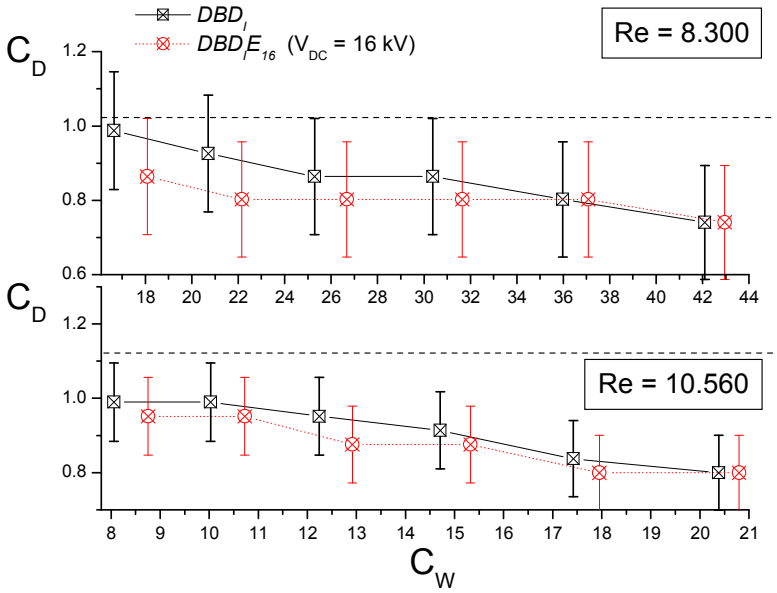

Figure 9. Drag coefficient (C_D) as a function of the power coefficient (C_W) for the *DBD* and *DBDE* actuators (with V_{DC} = 16 kV). (upper) Re = 8300 and (lower) Re = 10.560.

The horizontal dash line ($C_D = 1.1$) represent the drag coefficient in the base flow (i.e. without plasma actuation). We observe that a considerable drag reduction can be achieved with both types of actuators. The plotted curves $C_D(C_W)$ has a very small negative slope and the curves corresponding to the *DBDE* actuation (dot lines) always appear below (or almost equal to) the curves associated to the *DBD* actuation (solid lines). This trend was also observed within all the C_W and *Re* studied ranges.

Another important parameter to compare the actuators performances is the actuator efficiency (η) defined as:

$$\eta = \frac{\left(F_D{}^{OFF} - F_D{}^{ON}\right)U_0}{P} \tag{4}$$

Where $F_D{}^{ON}$ and $F_D{}^{OFF}$ are the cylinder drag force with and without plasma actuator respectively. The actuator efficiency evaluates the ratio between the power saved as a consequence of the drag reduction ($\left(F_D{}^{OFF} - F_D{}^{ON}\right)U_0$) and the electrical power required to energise the actuator (*P*).

Figure 10 shows the actuator efficiency (η) as a function of the power coefficient (C_W) for different Reynolds numbers. In this case we have compared the efficiency of the *DBD* actuators with that of the *DBDE* actuators with V_{DC} = 16 kV (DBD_IE_{16}).

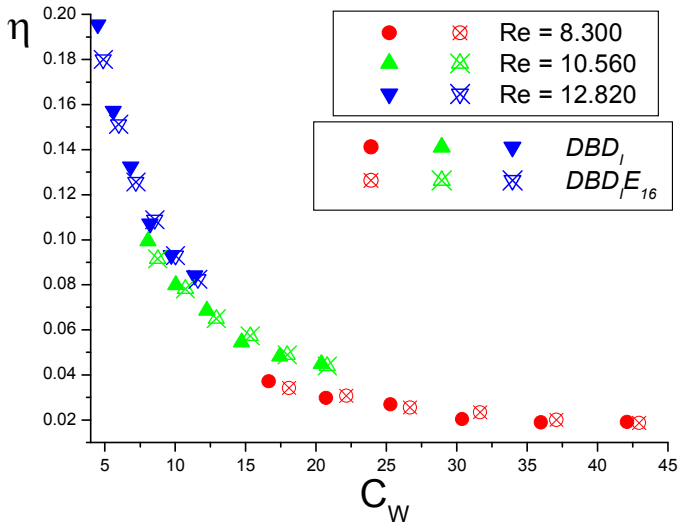

Figure 10 shows the DBD_I and DBD_IE_{16} (*DBDE* with V_{DC} = 16 kV) actuators efficiency (η) as a function of the power coefficient (C_W) for different *Re* numbers

This figure hides in some sense that the *DBDE* actuation enables to improve efficiency of *DBD* actuators as we expected from our previous experimental results. In fact for the same power coefficient (C_W) we have observed a higher momentum addition and higher drag reduction when a *DBDE* actuation was considered (see figure 6 and 9 respectively) and consequently the expected *DBDE* efficiency must be higher than the *DBD* ones. However the differences between the drag reduction achieved with the different kind of actuators (see figure 9) are not enough to revel this behaviour when these non-dimensional parameters are considered.

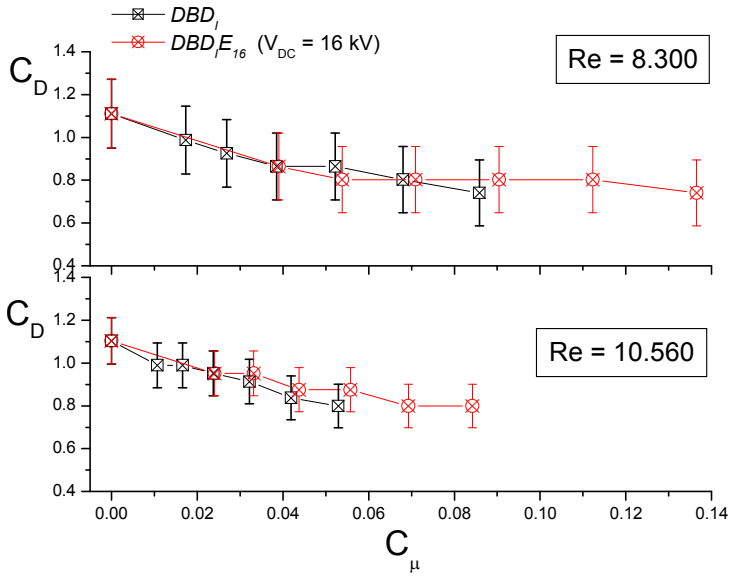

Figure 11. Drag coefficient (C_D) as a function of the momentum coefficient (C_μ) for the *DBD* and *DBDE* actuators (with V_{DC} = 16 kV). (upper) Re = 8300 and (lower) Re = 10.560.

In this figure it can also be observed that the actuator efficiency tends to diminish (for both kinds of actuators) when momentum coefficient increase. This efficiency reduction could be explained in terms of a saturation of the actuation with the increase in C_μ.

In Figure 11 we represent the drag coefficient (C_D) as a function of the momentum coefficient (C_μ) for the *DBD* and *DBDE* actuators for a typical case.

This figure enables to show that the increase in the momentum coefficient produce a similar decrease in the drag coefficient for both kinds of actuators. However for values of C_μ higher than $C_\mu \approx 0.06$ the drag coefficient seems to reach a saturation value. The actuator efficiency decreases for higher values of C_μ is in concordance with this saturation in the actuation (i.e. a saturation in the achievable increase of the $\left(F_D{}^{OFF} - F_D{}^{ON}\right)$ value for a fixed *Re* number). In other words for the higher C_μ values the consumed electrical power increase without a noticeable increase in the cylinder drag reduction. This plateau in the function $C_D\left(C_\mu\right)$ as been theoretically predicted by an analytical study of a tangential wall jet applied to the control of separated flow past a circular cylinder[40].It has been shown that the wall jet is very efficient in reducing drag by delaying the separation point in the range of small blowing strength because the suction force induced by the wall jet is negligible compared to the drag due to the external stream. However when the blowing strength is large this suction force finally produces an increase of the drag [40].

4. Conclusions

The drag reduction in a circular cylinder was explored by means of a novel three electrode plasma actuator (*DBDE*). The *DBDE* actuator can reduce the drag coefficient up to a ~25% respect to the base flow drag coefficient. It has been demonstrated that, within the present experimental conditions, the *DBDE* actuator, for a fixed value of the power coefficient, adds a higher momentum to the flow and, consequently, produces a higher drag reduction than the *DBD* actuator with the same power coefficient. For the flow configuration considered the characteristics of the actuation mechanism itself (steady momentum addition) is rather inefficient and it is very difficult to increase the drag reduction by increasing the amount of momentum due to the very small slope in the curves $C_D\left(C_\mu\right)$. For both kind of actuators the device efficiency has been analysed in terms of the power added to the flow. It has been found that the efficiency attained similar values of almost 20% but at high levels of actuation the efficiency reduced to a much lower level of 2 %. This saturation has been also observed with syntethic jets devices where it has been shown that the steady injection of momentum reduce the drag coefficient but when higher values of the momentum coefficient were considered the drag reduction reached a plateau and the efficiency actuator consequently decayed.

In the case under study the *DBDE* actuator does not increase appreciably the actuation efficiency respect to that achieved with *DBD*. However to produce similar levels of actuation both kind of actuators require different values of V_{AC} voltages (always lower for *DBDE*). The reduction in this high voltage value is highly beneficial as is directly related to: a lower instantaneous electrical power requirement (i.e. the electrical reactive power is lower), a reduction in the dielectric breakdown probability and a reduction in the leakage currents (which are produced by loss of insulation at high voltage and frequencies).

The work was done as a first proof of concept of *DBDE* actuators as efficient tools to govern the flow around bluff bodies. Presently we are working on unsteady actuation, which seems to hold even more promise than steady devices in matters of efficiency.

Acknowledgement
This work has been undertaken with ANPCYT grant PICT 38070 and UBACYT grant number I017

References

[1] Lin J, Towfighi J and Rockwell D 1995 Near-wake of a circular cylinder: control by steady and unsteady surface injection *J. Fluids Struct.* **9** 659–69
[2] Sevilla A and Martinez-Bazan C 2004 Vortex shedding in high Reynolds number axisymmetric bluff-body wakes: local linear instability and global bleed control *Phys. Fluids* **16** 3460–69
[3] Arcas D and Redekopp L 2004 Aspects of wake vortex control through base blowing/suction *Phys. Fluids* **16** 452–56
[4] Poncet P 2004 Topological aspects of three-dimensional wakes behind rotary oscillating cylinders *J. Fluid Mech.* **517** 27–53
[5] Choi S, Choi H and Kang S 2002 Characteristics of flow over a rotationally oscillating cylinder at low Reynolds number *Phys. Fluids* **14** 2767–77
[6] Cetiner O and Rockwell D 2001 Streamwise oscillations of a cylinder in a steady current. Part 1: locked-on states of vortex formation and loading *J. Fluid Mech.* **427** 1–28
[7] Blackburn H and Henderson R 1999 A study of two-dimensional flow past an oscillating cylinder *J. Fluid Mech*. **385** 255–86
[8] Carberry J, Sheridan J and Rockwell D 2003 Controlled oscillations of a cylinder: a new wake state *J. Fluids Struct.* **17** 337–43
[9] Amitay M, Smith B L and Glezer A 1998 Aerodynamic flow control using synthetic jet technology *36th AIAA Aerosp. Sci. Meet. Reno Nev. AIAA Pap. No.* 98–0208
[10] Glezer A and Amitay M 2002 Synthetic jets *Annu. Rev. Fluid Mech*. **34** 503–29
[11] Moreau E 2006 Airflow control by non-thermal plasma actuators *J. Phys. D: Appl. Phys*. **40** 605-636
[12] Sosa R Mecanismos de Acople en actuadores EHD PhD Thesis University of Buenos Aires Faculty of Engineering October 2007 (in Spanish)
[13] Scherbakov A et al 2000 Drag reduction by ac streamer corona discharges along a wing-like profile plate *AIAA Paper No* 2000-2670
[14] Roth J R, Sherman D M and Wilkinson S P 2000 Electrohydrodynamic flow control with a glow discharge surface plasma *AIAA J*. **38** 1172–9
[15] Jukes T N, Choi K S, Jonhson G A and Scott S J 2004 Turbulent boundary layer control for drag reduction using surface plasma *AIAA Meeting Portland USA paper* #2004-2216
[16] Corke T C, Mertz B and Patel M P 2006 Plasma flow control optimized airfoil *AIAA Meeting Reno USA paper* #2006-1208
[17] Roupassov D V, Zavyalov I N and Starikovskii A Y 2006 Boundary lauer separation plasma control using low-temperature non-equilibrium plasma of gas discharge *AIAA Meeting Reno USA paper* #2006-373
[18] Sung Y, Kim W, Mungal M G and Cappeli M A 2006 Aerodynamic modification of flow bluff objects by plasma actuation *Exp. Fluids* **41** 479–86
[19] Forte M, Jolibois J, Pons J, Moreau E, Touchard G and Cazalens M 2007 Optimization of a dielectric barrier discharge actuator by stationnary and non-stationnary measurements of the induced flow velocity: application to airflow control *Exp.Fluids* **43** 917-928
[20] Moreau E, Leger L and Touchard G 2006 Effect of a DC surface non-thermal plasma on a flat plate boundary layer for airflow velocity up to 25m/s *J. Electrostatics* **64** 215–25
[21] Artana G, D'Adamo J, Leger L, Moreau E and Touchard G 2002 Flow control with electrohydrodynamic actuators *AIAA J*. **40** 1773–9
[22] Artana G, Sosa R, Moreau E and Touchard G 2003 Control of the near wake flow around a circular cylinder with electrohydrodynamic actuators *Exp. Fluids* **36** 580–8
[23] Sosa R and Artana G 2006 Steady control of laminar separation over airfoils with plasma sheet

actuators *J. Electrostat*. **64** 604–10
[24] Sosa R, Moreau E, Touchard G and Artana G 2004 Stall control at high angle of attack with periodically excited EHD actuators *AIAA Oregon AIAA Paper No* 2004-2738
[25] Sosa R, Artana G, Moreau E and Touchard G 2007 Stall control at high angle of attack with plasma sheet actuators *Exp.Fluids* **42** 143-167
[26] Magnier P, Dunpin Hong, Leroy-Chesneau A, Pouvesle J M and Hureau J 2007 A DC corona discharge on a flat plate to induce air movement *J. Electrost.* **65** 655-659
[27] Magnier P, Dunpin Hong, Leroy-Chesneau A, Bauchire J M and Hureau J 2007 Control of separated flows with the ionic wind generated by a DC corona discharge *Exp. Fluids* **42** 815–825
[28] Léger L, Moreau E and Touchard G 2002 Effect of a DC corona electrical discharge on the airflow along a flat plate *IEEE Trans. Indust. Appl*. **38** 1478–85
[29] Louste C, Artana G, Moreau E and Touchard G 2005 Sliding discharge in air at atmospheric pressure: electrical properties *J. of Electrostat*. **63** 615-620
[30] Moreau E, Loustea C and Touchard G 2008 Electric wind induced by sliding discharge in air at atmospheric pressure *J. of Electrost*. **66** 107-14
[31] Moreau E, Sosa R and Artana G 2008 Electric wind produced by surface plasma actuators: a new dielectric barrier discharge based on a three-electrode geometry *J. Phys. D. Appl. Phys*. **41** 115204
[32] Sosa R, Arnaud E, Memin E and Artana G 2008 Study of the Flow Induced by a Sliding Discharge *IEEE Transactions on Dielectrics and Electrical Insulation* In press
[33] Asghar A and Jumper E J 2004 Phase synchronized of vortex shedding from two side-by-side circular cylinders using plasma actuators *AIAA Meeting Portland, USA paper* #2004-925
[34] McLaughlin T E, Munska M D, Vaeth J P, Dauwalter T E, Goode J R and Siegel S G 2004 Plasma-based actuators for cylinder wake vortex control *AIAA Meeting Portland USA paper* #2004-2129
[35] Thomas F O, Kozlov A and Corke T C 2006 Plasma actuators for bluff body flow control *AIAA Meeting San Francisco USA paper* #2006-2845
[36] Yadav, Manish Dai, Xin and Roth J R 2004 Measurement of the Boundary Layer Velocity Induced by Paraelectric Plasma Actuators using an Inexpensive High Voltage Power Supply *Proc. 31st IEEE Int. Conference on Plasma Science Baltimore Maryland Page 244, IEEE Catalog No.* 04CH37537, ISBN 0-7803-8334-6.
[37] Jacob J, Rivir R and Carter C 2004 Boundary layer flow control using AC discharge plasma actuators *AIAA 2nd Flow Control Meeting Portland Paper* 2004-2128
[38] Pons J, Moreau E and Touchard G 2005 Asymetric surface dielectric barrier discharge in air at atmospheric pressure:electrical properties and induced airflow characteristics *J. Phys. D: Appl. Phys*. **38** 3635-42
[39] Boucinha V, Magnier P, Leroy-Chesneau A, Weber R, Joussot R, Dong B and Hong D 2008 Characterization of the Ionic Wind Induced by a Sine DBD Actuator used for Laminar-to-Turbulent Transition Delay *AIAA Meeting Seatle USA paper* #2008-4210
[40] Oh S and Roberts L Control of separated flow past a cylinder using tangential wall jet blowing 1989 *JIAA TR-93*